Supplementary Information (SI) for Journal of Materials Chemistry A.

Support Information

Interface and Interlayer Electron/Exciton-Phonon Coupling of TMDs/InSe for Efficient Charge Transfer and Ultrafast Dynamics: Implications for Field-Effect Devices

Shan-Shan Kan[1], Shi-Xuan Deng[1], Xiao-Meng Jiang[1], Yu-Xin Liu[1], Ming-Kun Jiang[1], Zhe-Kun Ren[1], Cheng-Bao Yao[1,*]

[1]Key Laboratory of Photonic and Electric Bandgap materials, Ministry of Education, School of Physics and Electronic Engineering, Harbin Normal University, Harbin, 150025, Heilongjiang Province, China

**Corresponding author：yaochengbao5@163.com*

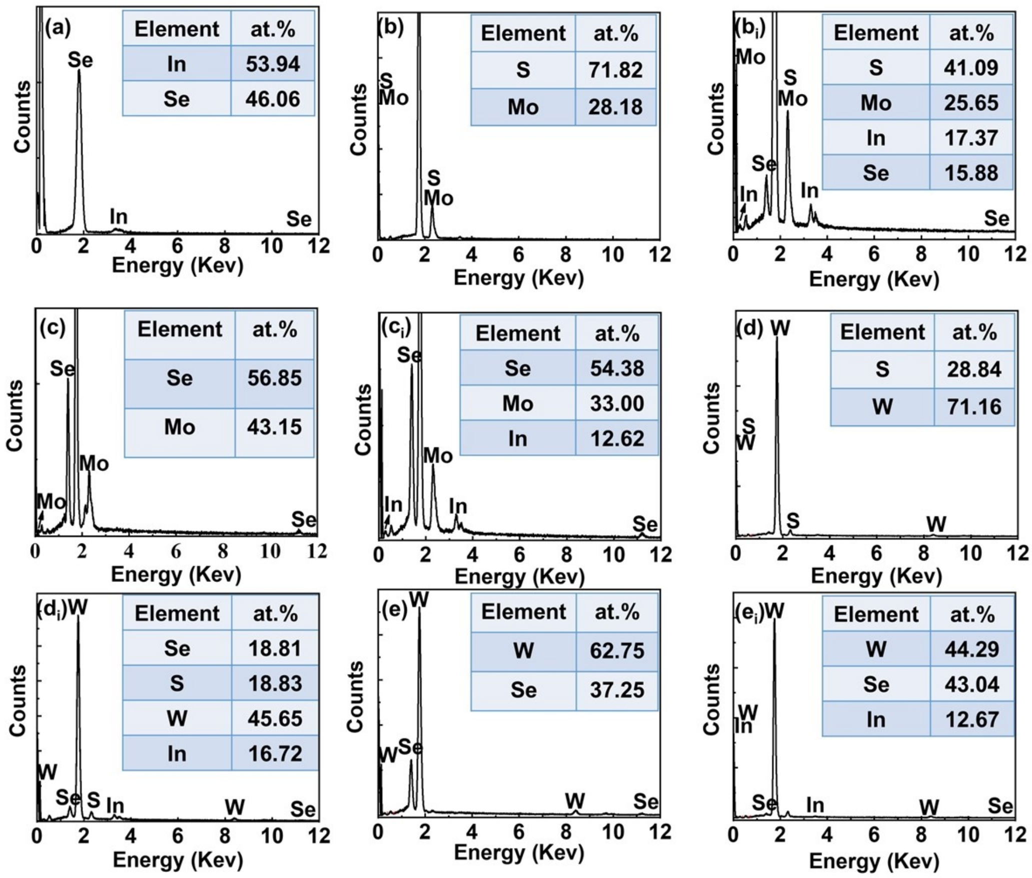

Fig. S1 EDS images of InSe (a), MoS_2 (b), $MoSe_2$ (c), WS_2 (d) and WSe_2 (e), and EDS images of MoS_2/InSe (b_i), $MoSe_2$/InSe (c), WS_2/InSe (d_i) and WSe_2/InSe (e_i).

Tab. S1 Detailed summary of XRD data for samples.

Phase	Peak (deg)	Planes	D (nm)	JCPDS
MoS_2	28.5	(004)	3.1325	75-1539
	39.5	(103)	2.2789	
	58.9	(008)	1.5662	
$MoSe_2$	13.7	(002)	6.4600	29-914
	31.5	(100)	2.8450	
	58.0	(112)	1.5910	
	69.5	(203)	1.3510	
WS_2	29.0	(004)	3.0890	8-237
	58.5	(008)	1.5458	
	75.9	(116)	1.2524	
WSe_2	13.6	(002)	6.5100	6-80
	27.4	(004)	3.2500	
	31.3	(100)	2.8500	
	59.7	(107)	1.5500	
	76.0	(205)	1.2500	
γ-InSe	10.6	(003)	8.3167	70-2541
	31.4	(015)	2.8456	
	59.3	(027)	1.5579	
ε-InSe	25.7	(100)	3.4650	34-1431
	32.2	(006)	2.7730	

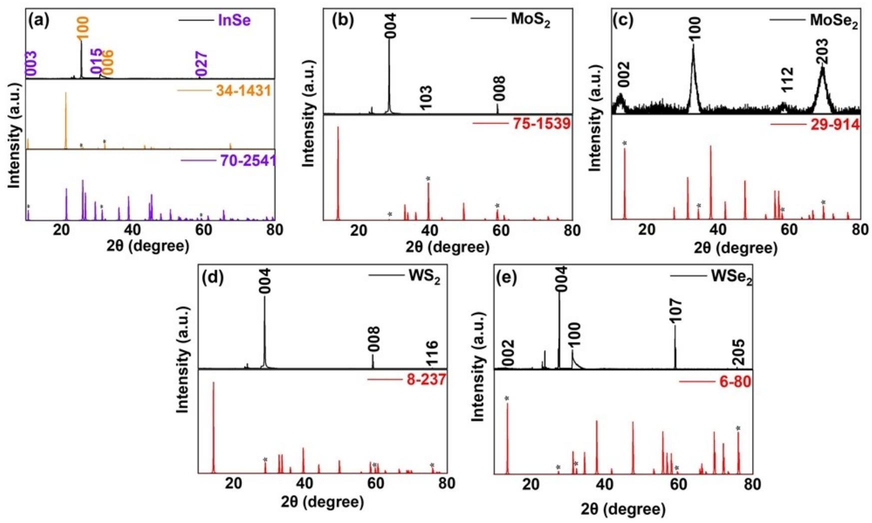

Fig.S2 XRD pattern and standard cards of InSe (a), MoS_2 (b), $MoSe_2$ (c), WS_2 (d), and WSe_2 (e)

(Among them, 34-1431 corresponds to hexagonal InSe, and 70-2541 corresponds to rhombohedral

InSe.).

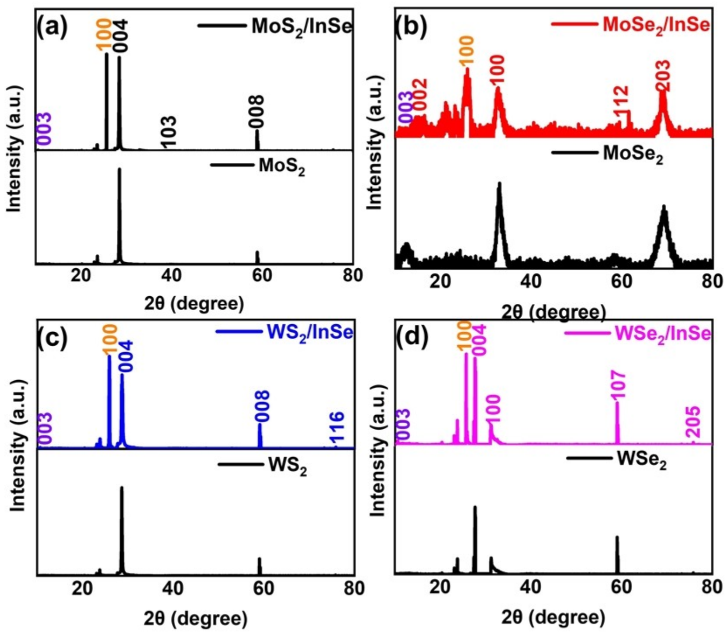

Fig.S3 XRD pattern of MoS_2/InSe and MoS_2 (a), $MoSe_2$/InSe and $MoSe_2$ (b), WS_2/InSe and WS_2 (c), and WSe_2/InSe and WSe_2 (d)

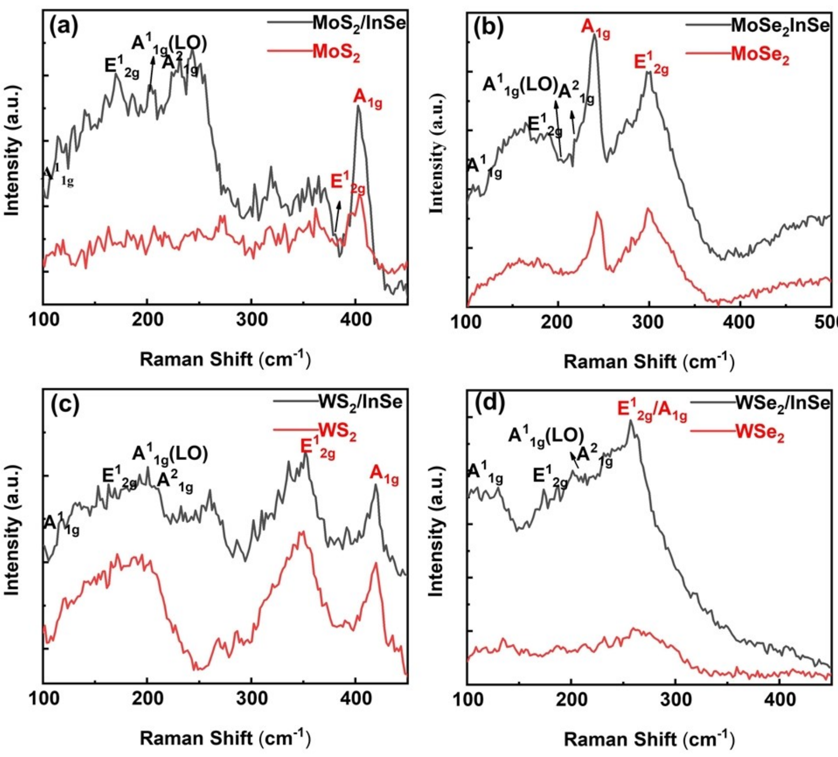

Fig. S4 Raman spectra of MoS_2/InSe and MoS_2 (a), $MoSe_2$/InSe and $MoSe_2$ (b), WS_2/InSe and WS_2 (c), and WSe_2/InSe and WSe_2 (e)

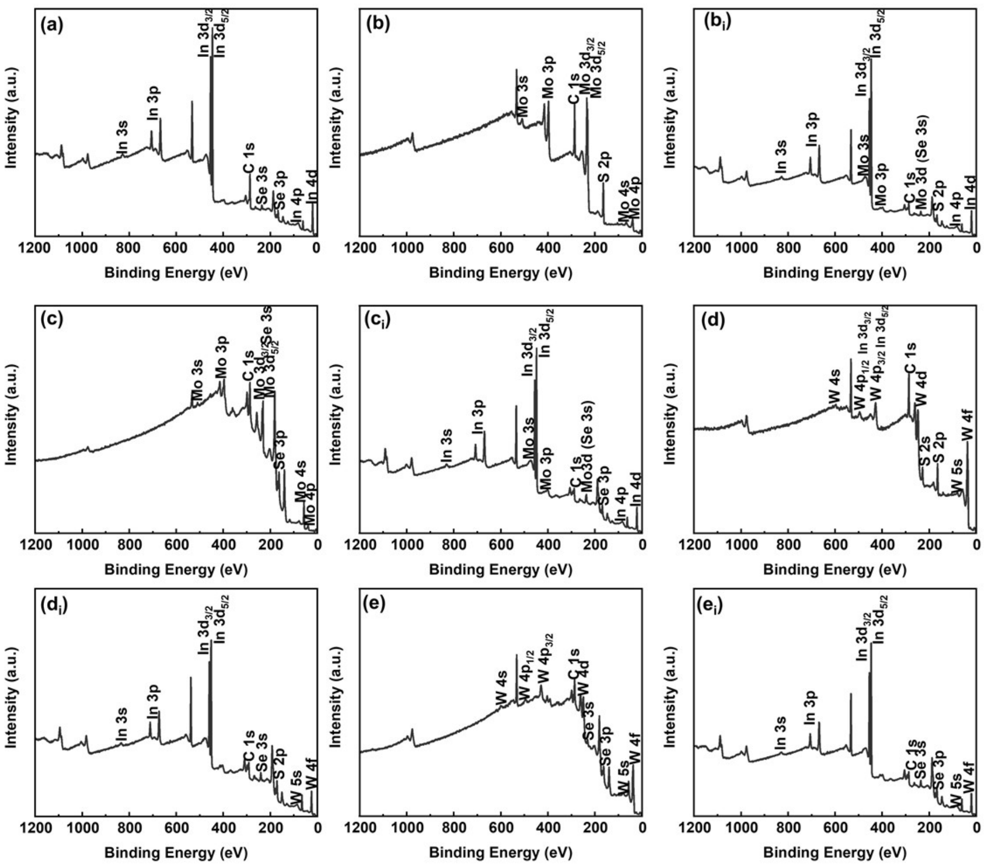

Fig. S5 Low-resolution XPS spectra of InSe (a), MoS_2 (b), $MoSe_2$ (c), WS_2 (d) and WSe_2 (e). Low-resolution XPS spectra of MoS_2/InSe (b_i), $MoSe_2$/InSe (c), WS_2/InSe (d_i) and WSe_2/InSe (e_i).

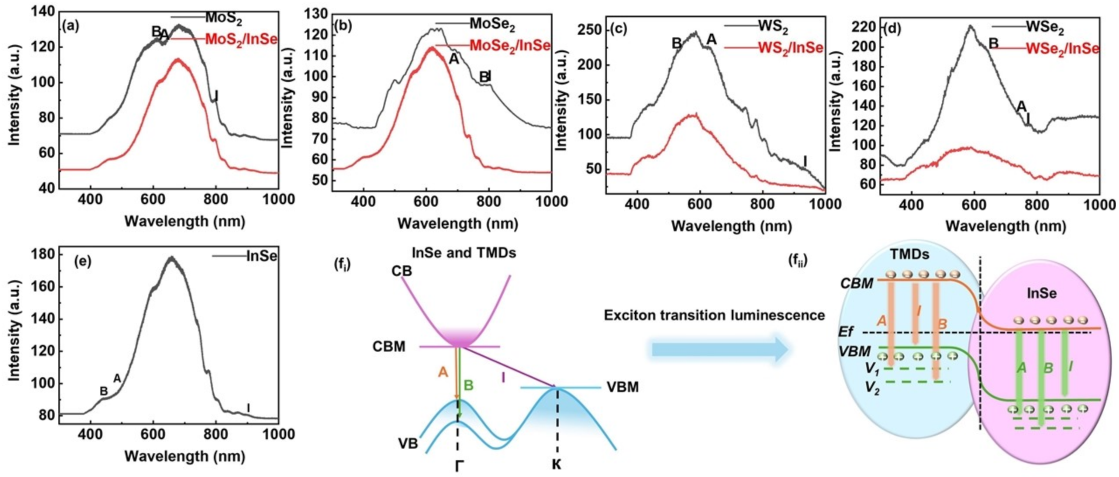

Fig. S6 PL spectra of TMDs and TMDs/InSe (a-d) InSe (e). (f_i) Exciton emission mechanism of InSe and TMDs. (f_{ii}) PL mechanism of TMDs/InSe heterojunctions.

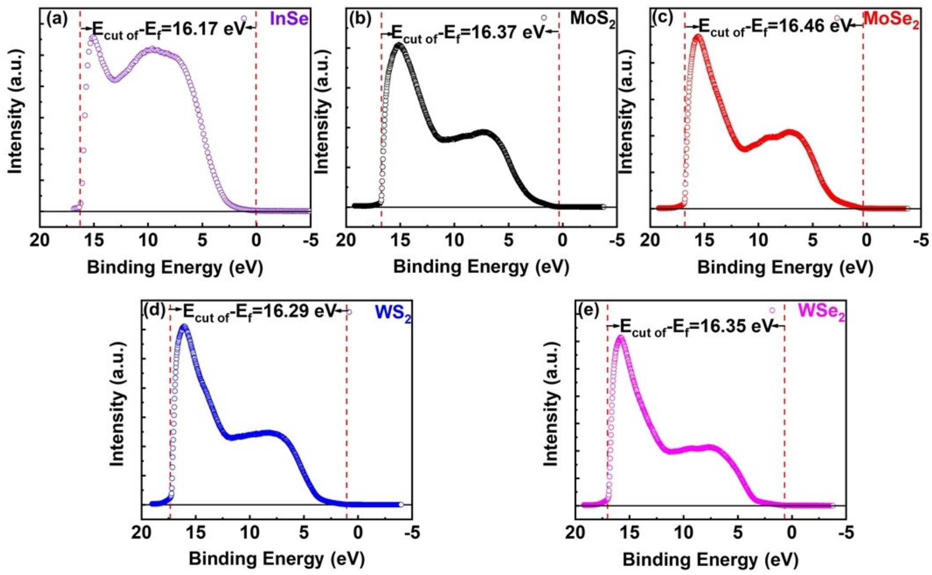

Fig. S7 UPS images of InSe and TMDs.

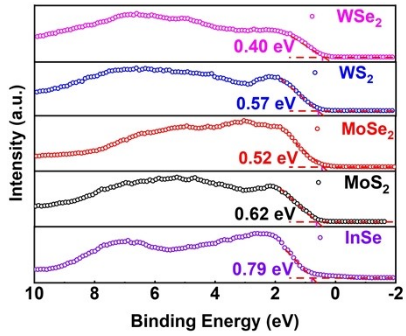

Fig. S8 VB spectra of InSe and TMDs.

Tab. S2. Time constants of A-exciton decay (monitored around 500 nm) of InSe and TMDs/InSe heterojunctions following 380 nm laser excitation.

	τ_1 (ps)	τ_2 (ps)	τ_3 (ps)
InSe	0.09	16.82	753.69
MoS_2/InSe	0.14	234.69	841.09
$MoSe_2$/InSe	0.12	19.82	778.66
WS_2/InSe	0.24	36.92	1256.70
WSe_2/InSe	0.69	235.59	1015.69

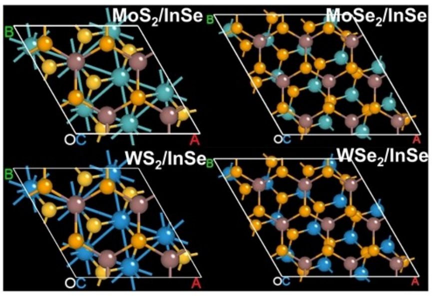

Fig. S9 TMDs/InSe heterojunctions atomic structure building model.

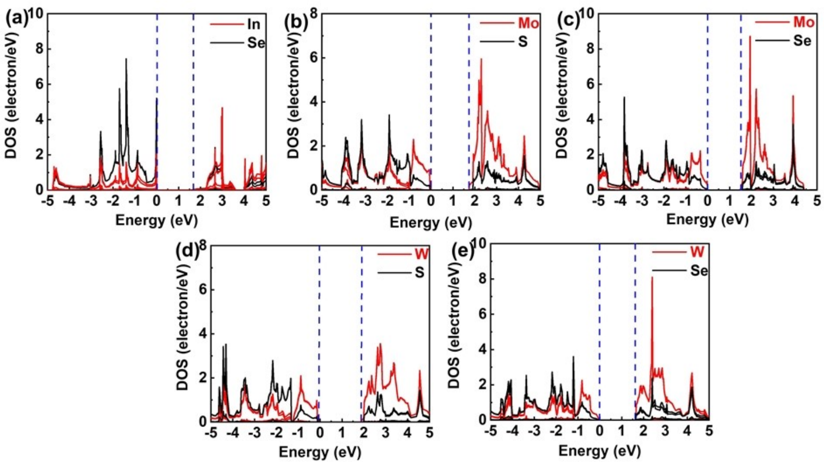

Fig. S10 PDOS of InSe (a), MoS_2 (b), $MoSe_2$ (c), WS_2 (d), and WSe_2 (e)

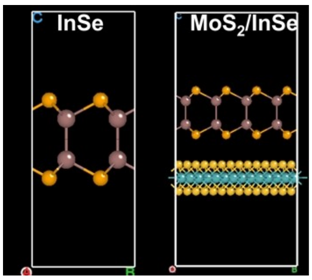

Fig. S11 Modeling of the calculated electron mobility of InSe and MoS_2/InSe heterojunction.

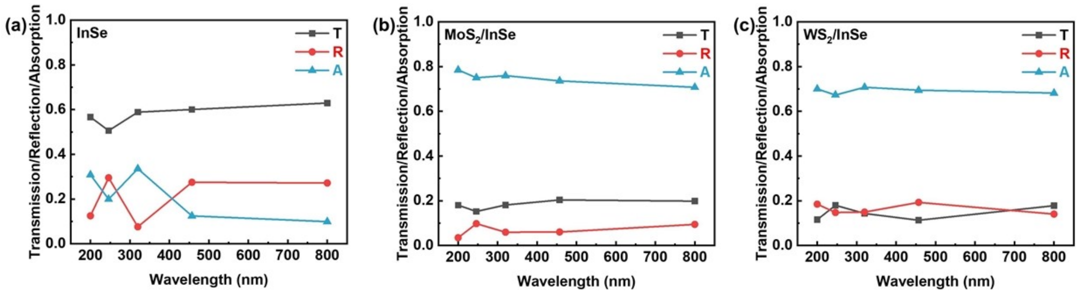

Fig. S12. Transmission, reflection, and absorption spectrum of InSe (a), MoS_2/InSe (b), and WS_2/InSe (c) heterojunctions films, respectively.

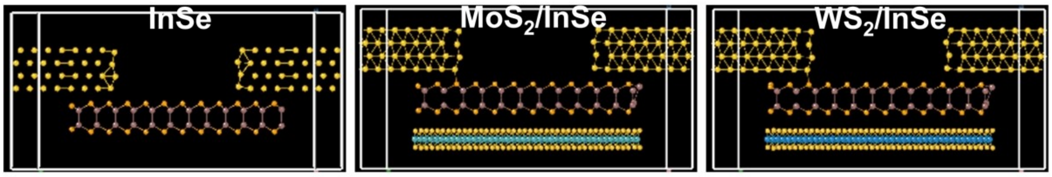

Fig. S13 Theoretical model of Au-InSe and MS_2/InSe heterojunctions electrodes.

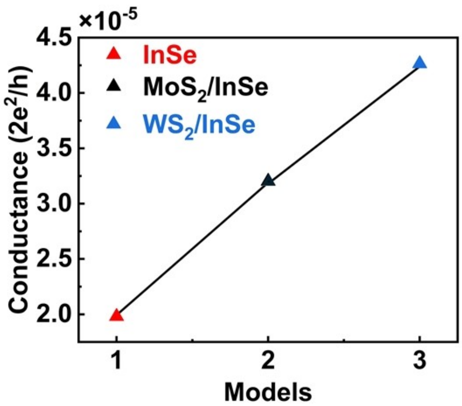

Fig. S14 Conductivity of InSe and MS_2/InSe heterojunctions transport devices.

Tab. S1 calculates the carrier effective mass m* (m_0), deformation potential E_1 (eV), planar stiffness C_{2D} (N/m), and electron mobility μ ($cm^2 \cdot V^{-1} \cdot s^{-1}$) of single-layer InSe and MoS_2/InSe heterostructures along the x and y directions at room temperature.

material	m_x^* (m_0)	m_y^* (m_0)	E_{1X} (eV)	E_{1y} (eV)	C_{2Dx} (N/m)	C_{2D-y} (N/m)	μ_x ($cm^2V^{-1}S^{-1}$)	μ_y ($cm^2V^{-1}S^{-1}$)
InSe	0.24	0.24	-6.67	-7.14	54.69	108.01	476	820
MoS_2/InSe	0.25	0.25	-2.33	-2.33	152.13	39.24	9730	2510

Tab. S4 For reference, we list some previous calculations of the electron mobility of TMDs at room temperature,[12, 53, 61] and experimental values.[13, 52, 62]

material	μ_x ($cm^2V^{-1}s^{-1}$)	μ_y ($cm^2V^{-1}s^{-1}$)	μ_{exp} ($cm^2V^{-1}s^{-1}$)	Ref.
MoS_2	271-285		——	12
$MoSe_2/MoS_2$	400-423		——	12
MoS_2	——	——	0.226	13
$ReSe_2$	——	——	0.226	13
$MoS_2/ReSe_2$	——	——	4	13
SnS_2	——	——	0.6	52
MoS_2	——	——	1.1	52
SnS_2/MoS_2	——	——	27.26	52
InSe	1995	1803	——	53
BP	1030	87	——	53
InSe/BP	2838	3670	——	53
InSe	1619.51	1779.16	——	61
Zr_2CO_2	57.55	612.12	——	61
$InSe/Zr_2CO_2$	10942.98	9293.66	——	61
InSe	——	——	10^3	62

Tab. S5 Carrier concentration, Hall mobility, and resistivity of InSe and MoS_2/InSe heterojunction.

	Carrier Concentration	Hall mobility	Resistivity (ρ)
InSe	1.727×10^{14} cm^{-3}	1.59×10^3 $cm^2V^{-1}S^{-1}$	22.67 Ωcm
MoS_2/InSe	$4.743\times10^{15}cm^{-3}$	$1.85\times10^3cm^2V^{-1}S^{-1}$	0.711 Ωcm